https://dx.doi.org/10.1016/j.ultras.2020.106289

Quantitative Characterization of the Colorectal Cancer in a Rabbit Model Using High-frequency Endoscopic Ultrasound

Cheng Liu,[*] Yaoheng Yang,[*] Weibao Qiu,[†] Yan Chen,[‡] Jiyan Dai,[‡] and Lei Sun[*]

[*] Department of Biomedical Engineering, The Hong Kong Polytechnic University, Hong Kong SAR, China, People's Republic of

[†] Paul C. Lauterbur Research Center for Biomedical Imaging, Shenzhen Institutes of Advanced Technology, Chinese Academy of Sciences, Shenzhen, China, People's Republic of

[‡] Department of Applied Physics, The Hong Kong Polytechnic University, Hong Kong SAR, China, People's Republic of

Please send correspondence to:

Lei Sun, Ph.D

Room ST409, Department of Biomedical Engineering,

The Hong Kong Polytechnic University,

Hong Kong SAR, China, People's Republic of.

Phone: (852) 2766 7663

Email: lei.sun@polyu.edu.hk

ABSTRACT

Purpose: Colonoscopy accompanied with biopsy works as the routine endoscopic strategy for the diagnosis of colorectal cancer (CRC) in clinic; however, the colonoscopy is limited to the tissue surface. During the last decades, enabling technologies are emerging to complement with the colonoscopy for better administration of CRC. The conventional low-frequency (<12 MHz) endoscopic ultrasound (EUS) guided fine-needle aspiration (FNA) has been widely used to assess the lesion penetration. With the high-frequency ultrasound transducer (>20 MHz), EUS allows more precise visualization of the colorectal abnormalities. In order to achieve the accurate detection or *in situ* characterization of the colorectal lesions, the EUS diagnosis needs more patho-physiological related information in the micro-structural or molecular level. Quantitative ultrasound (QUS) technique, which could extract the micro-structural information from the ultrasound radio-frequency (RF) signal, is promising for the non-invasive tissue characterization. To date, the knowledge of the high-frequency endoscopic QUS for the CRC characterization has not been fully determined.

Methods: In this work, to our best knowledge, it is the first application of the QUS technique based on a customized high-frequency EUS system (30.5 MHz center frequency) to characterize the colorectal malignancies in a VX2 rabbit CRC model. To eliminate the response from the ultrasound electronic system and transducer, the ultrasound signals from colon tissue were calibrated. And, the resulting quasi-liner ultrasound spectra were fit by the linear regression test. As a result, three spectral parameters, including the slope (k), intercept (I) and Midband Fit (M), were obtained from the best-fit line. The three spectral parameters were compared between the malignant tissue regions and adjacent normal tissue regions of the colon tissue specimen *ex vivo*.

The independent t-test was conducted between the three parameters from the normal and malignant group. The statistical method of Fisher Linear Discriminant (FLD) was used to explore the linear combinations of the three parameters, so as to provide more tissue micro-structural features than the single parameter alone. The three FLD values were derived from three different combinations among k, I and M. The threshold was selected from the statistical analysis to optimize the differentiation criteria between the malignant and the normal tissues. The color-coded images were used to display the local FLD values and combined with the EUS B-mode image.

Results and Conclusions: The mean Midband Fit (M) and intercept (I) showed significant differences between the malignant and normal tissue regions. The statistical analysis showed that there were significant differences in all the mean FLD values of the spectral parameter combinations (kI, kM and IM) (t test, $P < .05$). And, the combined image result from the B-mode image and color-coded image could visually correlate with the histology result. In conclusion, the high-frequency endoscopic QUS technique was potential to be used as a complementary method to distinguish the colorectal malignancies by leveraging its morphological and micro-structural ultrasound information.

Keywords: Quantitative ultrasound, endoscopic ultrasound, colorectal cancer, high-frequency ultrasound, spectral parameter analysis

INTRODUCTION

To date, the conventional endoscopy accompanied with biopsy works as the wide-spread routine endoscopic screening choice for the colorectal cancer (CRC) in clinic.[1] However, it is limited to evaluate the penetration of lesion invasion into the colorectal wall, which is a crucial factor for the CRC diagnosis.[2] During the last decades, technologies are emerging to complement with the conventional endoscopy to further improve the outcome of the clinical intervention, such as chromoendoscopy,[3] autofluorescence endoscopy,[4] confocal endoscopy,[5] OCT endoscopy,[6] two-photon endoscopy,[7] photoacoustic endoscopy[8] and wireless capsule endoscope.[9] Enabling imaging strategies are still demanding for better administration of the complications of colorectal cancer in the clinical or pre-clinical studies.

Due to the ability to identify the cross-sectional structures and adjacent organs, the conventional low-frequency (<12 MHz) endoscopic ultrasound (EUS) guided fine-needle aspiration (FNA) has been accepted as one standard method to assess the colorectal lesion penetration depth and evaluate the structural alternations of the adjacent organs. The recent studies have shown that at higher frequency (>20 MHz) the EUS is able to delineate the mucosa and submucosa layers of the normal human colorectal wall relying on the morphological imaging. Therefore, it allows more precise visualization of the colorectal abnormalities at the high frequency range.[10,11] The images obtained with the mini high-frequency ultrasound probe working in the operation channel of the colonoscopy could provide additional depth information of the lesions through the layered colorectal structure. And, it could also determine the tumors that are only invasive to the layers of mucosa and submucosa.[12,13] The mini high-frequency ultrasound colonoscopic imaging technique has been proved to be a valid tool for clinical severity prediction in ulcerative colitis of the rectum.[2]

And, it has been shown to be a promising diagnostic method for the colonic lesions in a mouse model of CRC, based on an ultrasound mini probe catheter working in the operation channel of a pediatric bronchofiberscope.[14]

In order to achieve the accurate detection or *in situ* characterization of the abnormal colorectal lesions, the EUS diagnosis needs more patho-physiological related information in the micro-structural or molecular level. The conventional B-mode EUS imaging can be generated by displaying the envelope amplitude of the back-scattered radio-frequency (RF) ultrasound signals. However, the images generated in this way are subjected to the loss of inherent tissue properties from the raw RF data. In addition, a variety of factors, including the electronic ultrasound system, ultrasound transducer and image post-processing algorithm, all render the B-mode images operator and system dependent.[15] Hence, to produce images that could represent the objective tissue properties and allow easy comparison of images obtained with different ultrasound systems, some novel methods need to be developed to eliminate or minimize these factors.

Quantitative ultrasound (QUS) is a promising technique for the non-invasive tissue characterization. In brief, the technique could extract the spectral properties from the back-scattered RF ultrasound signals, which could be processed to generate the quantitative estimates associated with the tissue micro-structure, including the effective scatter size, acoustic concentration, intercept and slope. To date, this spectrum-based imaging technique has been investigated by some pioneers. The correlation relationship between the spectral parameters and the tissue characterizations has been studied in some different applications, such as prostate cancer,[16–19] breast cancer,[20] ocular cancer,[21] lymph node metastases,[22–24] liver disease,[25,26]

intravascular plaque,[27,28] and cataract.[29,30] Nevertheless, the knowledge of the high-frequency endoscopic QUS technique for the CRC characterization has not been determined yet.

In this work, it was hypothesized that the spectral parameters derived from the back-scattered high-frequency RF ultrasound signals could be used to distinguish the colorectal malignancies. To the best of our knowledge, this was the first application of the QUS technique, based on a customized high-frequency endoscopic ultrasound (EUS) system,[31–33] to characterize the malignant and normal colorectal tissues, in a rabbit model of CRC. The research purpose was to explore the potential of the high-frequency endoscopic QUS technique to distinguish the CRC, by combining the complementary QUS image with the B-mode EUS morphological image. In particular, the rabbit CRC model was used, for the first time, as a reproducible animal model for the studies of the high-frequency endoscopic QUS technique.

MATERIALS AND METHODS

A flexible high-frequency EUS platform was designed for potential applications in endoscopic imaging. The design diagram of the platform is illustrated in **Fig. 1**. A side-view single element endoscopic ultrasound transducer was used to transmit and receive depth-resolved ultrasound echo signals in depth orientation. 2D transverse ultrasound images could be acquired by driving the

Customized Endoscopic Ultrasound (EUS) System

In our preliminary work, a customized high-frequency imaging system has been developed for real-time EUS applications,[33–35] as shown in **Fig. 1**. This compact system, which was based on the cost-effective electronic components and PCB board, was designed to implement the reconfigurable hardware circuitry, programmable algorithms and RF data acquisition. The system employed a high-performance FPGA microprocessor to achieve real-time imaging. Low noise electronic components were selected to support the large signal-to-noise ratio (SNR) and precise data acquisition. A mini single element side-view transducer (PMN-0.28PT based, 70 μm thick, 0.9 mm × 0.9 mm, 30.5 MHz center frequency, -6 dB bandwidth = 30.7%) was employed. In particular, the stored raw RF data in real-time was used for the further quantitative data processing. The algorithms for the quantitative ultrasound (QUS) processing could be implemented into this compact system by software configuration. More details of the customized high-frequency transducer and EUS system were introduced in our previous works.[31,32]

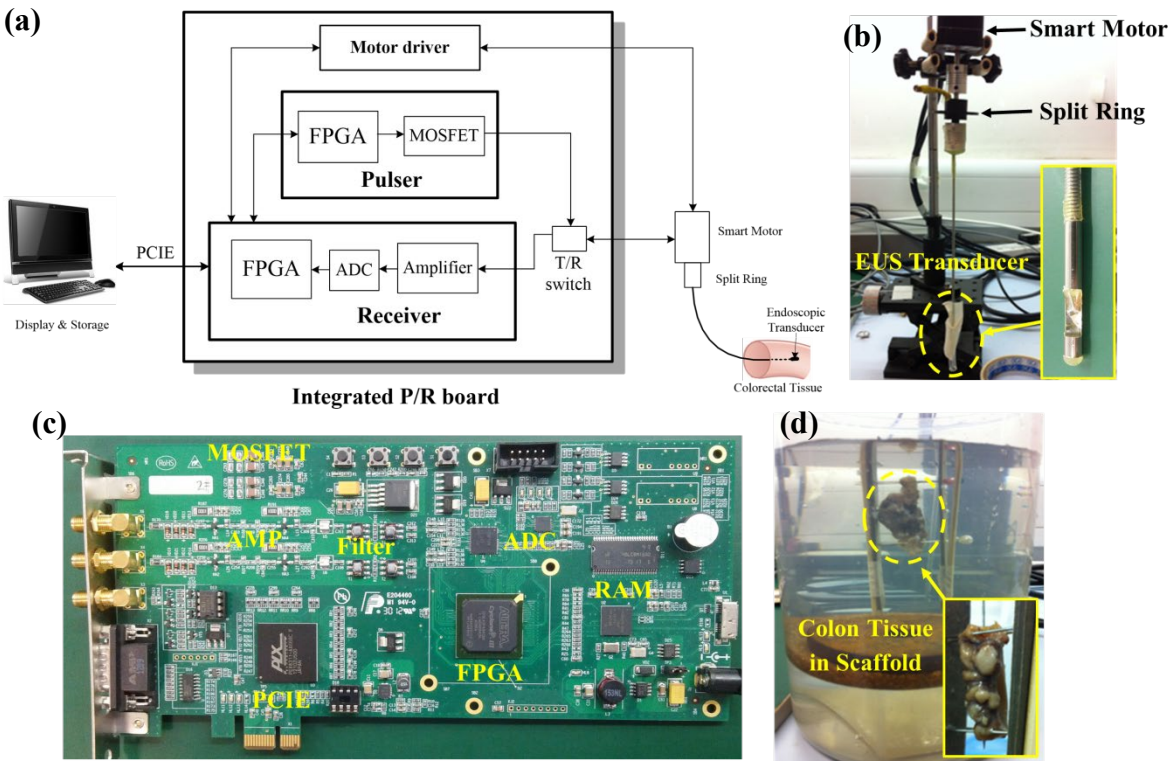

Fig. 1. (a) Design diagram of the high-frequency EUS platform;[33] (b) ultrasound signal acquisition setup with the smart motor and high-frequency endoscopic transducer with a split ring; (c) the customized high-frequency EUS system (PCB board); (d) photographs of *ex vivo* malignant colon segment immersed in a water tank. The colon segment was immobilized by a scaffold with four steel nails.

Rabbit Colorectal Cancer (CRC) Model

All the animal experiments were undertaken in the Centralised Animal Facilities of the Hong Kong Polytechnic University under an ethical protocol which was approved by the Department of Health, the government of the Hong Kong Special Administrative Region and the University's Animal Subjects Ethics Sub-committee.

To date, the animal models of colorectal carcinoma are often induced by chemical carcinogens, which require excessive time and induce large individual variations. In our experiment, the VX2 cell line (National Infrastructure of Cell Line Resource, Chinese Academy of Science, Shanghai, China), which is the only tumor cell line for the rabbit tumor models of unspecified tissue origin, was used for the rabbit colorectal implantation. The trans-abdominal implantation was conducted with the technical support from the Guangdong Provincial Clinical Animal Experiment Center.

In this work, six male New Zealand White rabbits at 4-5 months old, weighting 2.5-3.5 kg were used. The animals were fed with a pellet diet and free access to distilled water. The experimental rabbits were lavaged 24 hrs prior to the implantation. Before the trans-abdominal implantation, the rabbits were anesthetized with 30 mg/kg pentobarbital sodium *via* the ear vein. The rabbits were kept at a supine position with their four legs fixed during the implantation. A total of 0.2 mL of VX2 cell suspension was injected into the colon, followed by injection of 0.1-0.2 mL of normal sodium to fully rinse the VX2 cells into the colon wall. After 5 mins, the needle was withdrawn slowly. The rabbits were allowed to access normal food after recovery from anesthesia. After two-week growth, the rabbits were sacrificed by injecting 3.0 mL/kg of euthanasia solution Tanax®(T-61) *via* the ear marginal vein. Then, a 20 cm segment of colon tissue containing tumor between the appendix and the ileo-cecal valve was rapidly excised for the *ex vivo* data acquisition experiment.

Ultrasound Signal Acquisition Setup

The colon segment containing tumor site was immobilized in a scaffold by four steel nails, two in the cephalad edge and two in the caudal edge. The function of the 4 nails was not only to

immobilize the colon segment but also to expand the inner space of the colon segment to ensure enough space for the EUS scanning, as shown in **Fig. 1**. Before the EUS scanning, the location of the tumor site to the two edges of colon segment was recorded, which was used to guide the EUS transducer to the tumor sites of interest. Finally, the high-frequency EUS system acquired and recorded the radio-frequency (RF) data for further quantitative ultrasound (QUS) data processing.

Quantitative Ultrasound (QUS) Data Processing

A QUS data processing program was developed according to the reported QUS analysis method.[36] Briefly, the QUS data processing program involved the following steps:

1) B-mode image construction

The B-mode ultrasound image was generated from the received RF signals through a series of processes, including 1) band-pass filtering, 2) envelop detection, 3) dynamic range transformation and 4) median filtering. The cutoff frequency of the band-pass filter was set to be 10 MHz in high pass and 65 MHz in low pass, respectively, which was used to restore enough back-scattered spectral information. The dynamic range was set to be 45 dB, because such dynamic range could recover the maximal structural information and maintain the relatively low noise. The median filter was applied to the envelope signal to reduce the speckle noise. The order of the median filter was evaluated on the basis of the trade-off between the residual speckle noise and the image quality. Finally, the order 3 median filter was selected.

2) Spectrum calibration

To remove the artifacts associated with the composite transfer function of the electronic ultrasound system and the transducer,[37] spectrum calibration was necessary for RF data processing. In this work, a glass plate was used as the calibration target plane because it could generate a significant acoustic impedance difference at the glass-water interface. The calibration target plane was ensured to be vertical to the transmission beam of the transducer. The distance between the transducer and the calibration target plane was set to be 3 mm, because the distance was close to that between the transducer and the rabbit colon segment wall. During the acquisition of calibration signals, the EUS transducer was kept steady instead of rotating, because the rotating transducer could not ensure normality to the calibration target plane. To reduce the experimental error, multiple calibration signals were recorded and averaged.

3) Spectral parameter calculation

To develop a database of spectral parameters, the back-scattered RF signals were classified into two groups, including normal group and malignant group. The regions of interest (ROIs) representing the two groups were selected from each scanning plane and recorded in the database for further processing. Every RF signal in a ROI was multiplied by the Hanning window (L=length of ROI) along the scanning line, and followed by the Fast Fourier Transformation (FFT). The mean of the squared spectral magnitude was calculated from the ensemble averaged power spectrum in the ROI.

$$S(f) = \left| FFT\left[RF_L(t) H_L(t) \right] \right|^2 \tag{1}$$

$$S_{ROI}(f) = \frac{1}{N} \sum_{i=1}^{N} S_i(f) \tag{2}$$

In Equation (1), the RF signal in a ROI was represented as $RF_L(t)$. The Hanning window function (L=length of a ROI) was represented as $H_L(t)$. In Equation (2), the averaged power spectrum function of a ROI was represented as $S_{ROI}(f)$. The averaged 1D power spectrum of the colon tissue segment was calibrated to correct for response from the electronic ultrasound system and transducer by dividing the averaged spectrum with the calibration spectrum. Finally, the calibrated spectrum was transferred to logarithmic form as:

$$W_{ROI}(f) = 10\log[S_{ROI}(f)] - 10\log[S_{cali}(f, z_{ref})] \quad (3)$$

Where:

$$S_{cali}(f, z_{ref}) = \frac{4}{R(f)^2}\left|FT\left[RF_{cali}(t, z_{ref})\right]\right|^2 \quad (4)$$

In Equation (3)-(4), the calibration signal from the glass-water interface at depth was represented as $RF_{cali}(t, z_{ref})$. And, the frequency-dependent pressure reflection coefficient of the glass-water interface was represented as $R(f)$. A linear regression was applied to the calibrated spectrum between 15 to 35 MHz. The fit line was calculated to obtain three spectral parameters, including slope (k) (dB/MHz), intercept (I) (dB) and Midband Fit (M) (dB). For ultrasound signals above 30 MHz, the attenuation in the water could not be neglected. The relationship between the theoretical parameters and practical parameters with the attenuation compensation was reported by pioneers in the field:[38,39]

$$I' = I \quad (5)$$

$$K' = K - 2\alpha X \quad (6)$$

234 $$M' = M - 2\alpha X f_c \quad (7)$$

235 The theoretical parameters without attenuation compensation were represented as intercept (I),
236 slope (k) and Midband Fit (M); and the practical parameters after the attenuation compensation
237 were represented as I', k' and M'. The acoustic attenuation coefficient, the depth of a ROI and the
238 center frequency were represented as α, X and f_c, respectively. According to Equation (5)-(7),
239 the intercept (I) was independent to the attenuation, while the practical parameters, including slope
240 (k) and Midband Fit M, were in linearity with their theoretical parameters.

241

242 **Statistical Analysis**

243 The independent t-test was conducted between the parameters from the normal and malignant
244 group in the database. The assumption of the t-test was that the two groups of data was normally
245 distributed. In preliminary work, pioneers in this field proved that the probability density function
246 (pdf) of the slope (k) and intercept (I) were Gaussian distributed in the histogram and Midband Fit
247 (M) had Gaussian pdf feature when the analysis spectral cells were more than 10.[38] In this work,
248 it was assumed that the slope (k), intercept (I) and Midband Fit (M) could be normally distributed.
249 The statistics software used in this work was IBM SPSS Statistics (Version 20).

250 Because only two of the three parameters were functionally independent, it was assumed that the
251 combinations of two parameters could provide more tissue micro-structural features than single
252 alone. The statistical method of Fisher Linear Discriminant (FLD) was employed to explore the
253 linear combination to distinguish the malignant and normal tissues. The application assumption of

FLD method was that the two compared groups were both normally distributed in the probability density function. The equation of FLD method was:

$$J_{fisher}(\varphi)=\frac{\varphi^T S_b \varphi}{\varphi^T S_W \varphi} \tag{8}$$

Where, φ represented the N dimension vector. The purpose of FLD method was to obtain Φ to maximize the value of $J_{fisher}(\varphi)$. Then, the two under-test parameters were projected to the vector φ. In Equation (8), the physical meaning was to find φ so that the two parameters which were projected to φ can have maximal value between class scatter (S_b) and minimal within class scatter (S_W). S_b and S_W were expressed as:

$$S_b=\sum_{i=1}^{c} P(i)(u_i-u)(u_i-u)^T \tag{9}$$

$$S_W=\sum_{i=1}^{c} P(i)E\left\{(u_i-x)(u_i-x)^T \,|\, x\in class\ i\right\} \tag{10}$$

In Equation (9)-(10), the u_i represented the mean value of class i; the $P(i)=\frac{n_i}{m}$ represented the probability of the sample that could fall into the class i.

$$W_{opt}=\arg\max\frac{\left|W^T S_b W\right|}{\left|W^T S_W W\right|} \tag{11}$$

In Equation (11), the optimization function to obtain a projection matrix W_{opt}, which was composed of a series of optimized discriminant vectors. W_{opt}, as a vector, was associated with the maximal value in following equation:

$$S_b \phi_i = \lambda S_W \phi \tag{12}$$

The calculated FLD value, which was related to the three different combinations among k, I and M, was analyzed by independent t-test between malignant group and normal group again to test the significance of difference.

Color-coded Image

The three FLD values were derived from three different combinations among k, I and M. The threshold was selected from the statistical analysis to optimize the differentiation criteria of the malignant from the normal tissues. The color-coded images were used to display the local FLD values. The color-coded images were formed by using a sliding Hanning window (0.5 mm) to progressively analyze the RF signal along the scanning line. At each window region, the averaged calibrated spectra (5 lines) were computed and corresponded to the local spectral parameters. Each FLD value from the three different combinations was projected to a FLD vector. The FLD values were coded with the differentiation criteria from the database. If the values fell into the malignant tissue band, the corresponding region was coded in red color; if normal tissue, it was coded in green color. Lastly, the color-coded image was combined with the original EUS image. The combined image could display the complementary morphological EUS and micro-structural QUS information.

Histology

After the EUS image scanning experiment, the colon tissues were cleaned and fixed in 4% formaldehyde for further paraffin embedding. The paraffin-embedded tissues were cross-sectioned (5 mm) stepwise transversally to the longitudinal axis of the colon tissue and stained with hematoxylin and eosin (H&E). All the stained sections of colon tissues were analyzed using light microscopy and compared with the image results for further analysis.

RESULTS

The B-mode image after the band-pass filtering and the median filter is shown in **Fig. 2**. In addition, the optimal dynamic range for the B-mode image was set to be 45 dB. The ultrasound echo with relatively strong amplitude was back-scattered by the interface with high acoustic impedance difference. A metal position marker was used to show the orientation of the colon tissue which was immobilized by the scaffold.

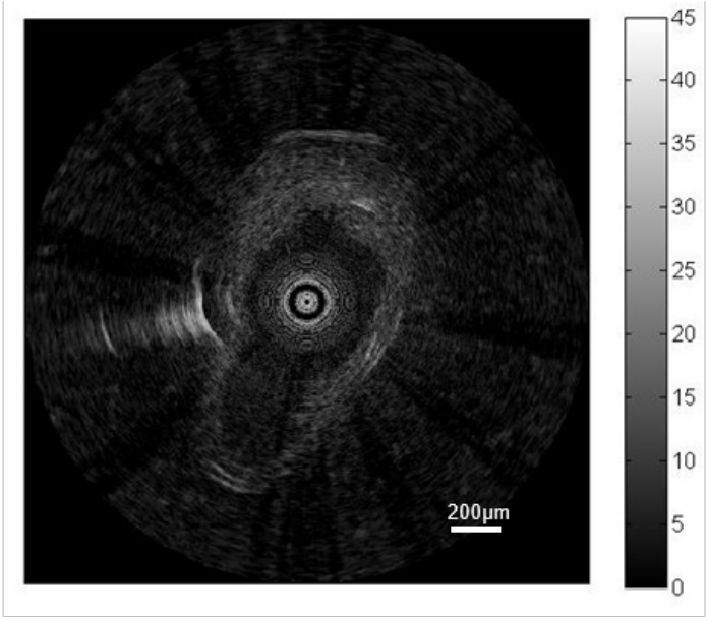

Fig. 2. The B-mode images after the band-pass filtering and median filtering.

The RF signal spectra of the normal colon tissue and the glass plate are shown in **Fig. 3(a)**. And, the best fitting line through the linear regression test to the calibrated spectrum in the frequency range of 15 to 35 MHz is shown in **Fig. 3(b)**.

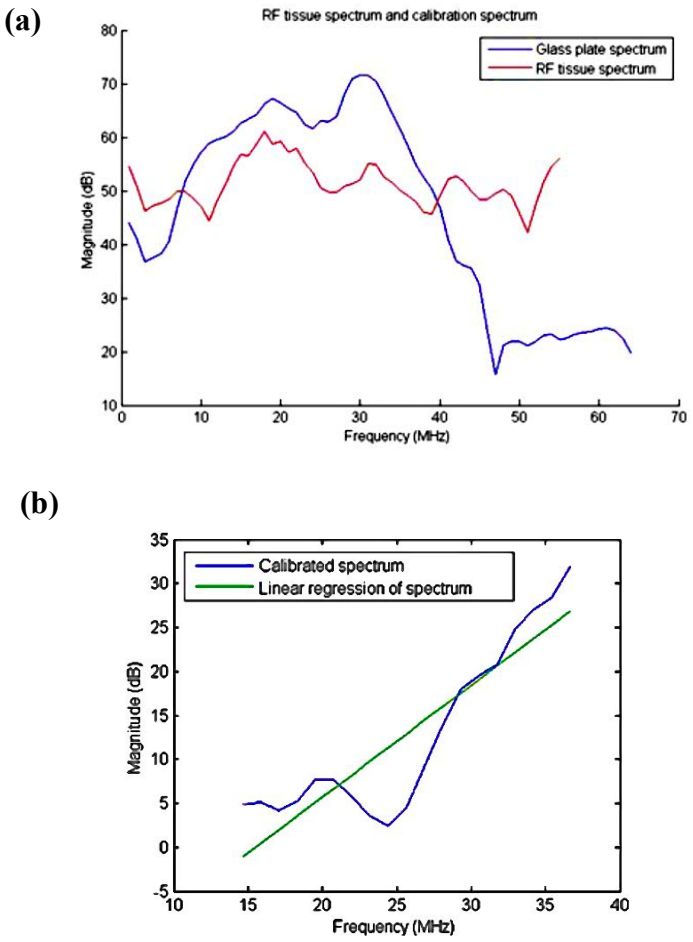

311

312

313 **Fig. 3.** (a) Plot of the RF signal spectra of the normal colon tissue and the glass plate plane. The
314 unstable spectrum shape was observed in RF signal spectrum before calibration. After calibration,
315 the useful signal to noise ratio (SNR) region was expanded to 15 to 35 MHz; (b) the best fitting
316 line from the linear regression test to the calibrated spectrum in the range of 15 to 35 MHz.

317

318 To develop a database of spectral parameters, the back-scattered RF signals were classified into
319 two groups, including normal group and malignant group. The regions of interest (ROIs)
320 representing the two groups were selected from each scanning plane and recorded in the database
321 for further processing, as shown in **Fig. 4**. The ROI size was standardized to be 0.63 mm in length

and 30 scanning lines in width. Totally, 90 ROIs for normal group and 79 ROIs for malignant group were selected from 13 different scanning planes, respectively.

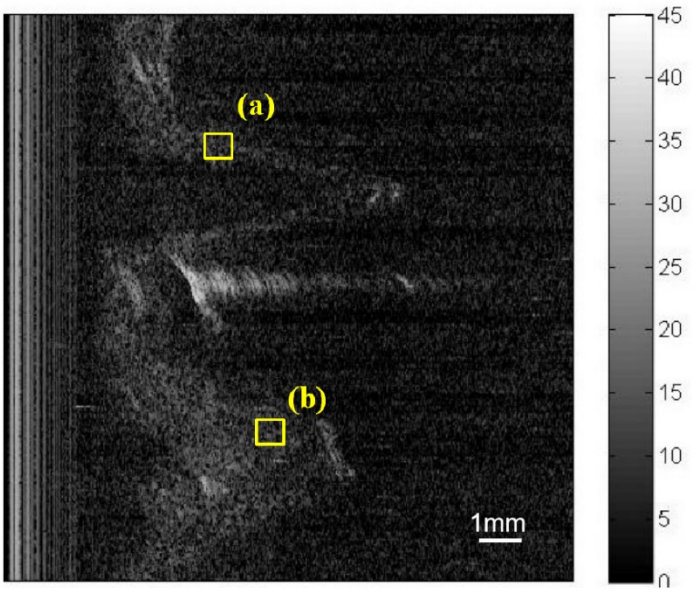

Fig. 4. The B-mode image in the Cartesian coordinate of colon segment with malignant tissue. The ROI in yellow color corresponding to (a) the normal tissue; (b) the cancer tissue.

After the spectrum analysis, the three spectral parameters (k, I, M) in the two groups were ready for further statistical analysis. The three spectral parameters were described in the means value and standard deviation (SD), as shown in Table I. Significant differences were found for spectral parameter intercept (I) ($p=0.024$) and Midband Fit (M) ($p<0.001$), while there was no significant difference ($p=0.334$) for the parameter slope (k).

Table I. The mean parameter values (k, I and M) of normal tissue group and cancer tissues group.

Tissue Type	Slope k (dB/MHz)	Intercept I (dB)	Midband Fit M (dB)
Normal tissue (n=90)	0.2857 ± 0.2279	-20.9525 ± 7.6356	-13.7966 ± 3.7113
Cancer tissue (n=79)	0.2342 ± 0.3368	-25.3867 ± 10.6543	-19.7522 ± 3.3587
Significant difference *	P = 0.334	P = 0.024*	P < 0.001*

335

336 The normal distribution map of the spectral parameter Midband Fit (M) and intercept (I) of the
337 normal tissue group and cancer group is shown in **Fig. 5**. On one hand, considering the normal
338 distribution map alone, the boundary value was hard to delineate. Therefore, neither the Intercept
339 (I) or the Midband Fit (M) alone was not be sensitive and specific enough to differentiate the
340 malignant tissue from normal tissue. On the other hand, because two parameters from the three
341 were independent, the combinations of two parameters were potential to provide more information
342 for the tissue characterization. Further statistical analysis regarding the mean value and standard
343 deviation (SD) was conducted to the FLD values for three different parameter combinations (kI,
344 kM and IM), as shown in Table II.

345

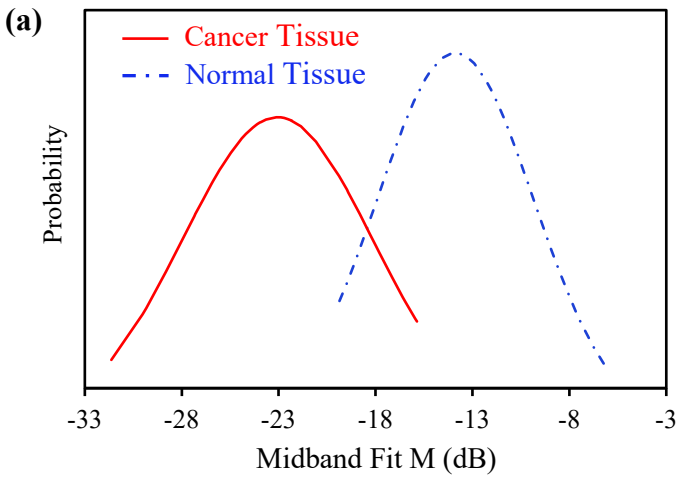

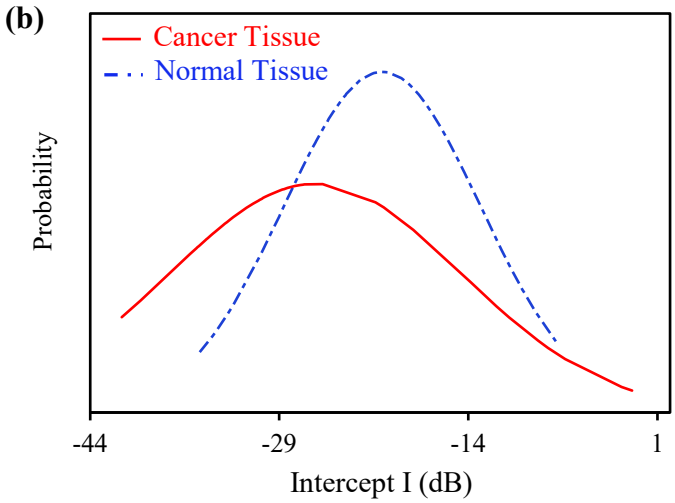

Fig. 5. The normal distribution map of (a) Midband Fit M, and (b) Intercept I between the cancer and normal tissue group. The red line and blue line represent the cancer tissue and normal tissue group, respectively.

As shown in Table II, all the mean FLD values for the three different parameter combinations showed significant difference ($p<0.001$).

354 Table II. The mean FLD values for the three different parameter combinations (kI, kM and IM).

Tissue Type	FLD value of kI	FLD value of kM	FLD value of IM
Normal tissue (n=90)	0.3826±0.1184	1.4828±0.4818	8.7329±2.7244
Cancer tissue (n=79)	0.5467±0.0752	2.3059±0.3527	12.9261±1.9431
Significant difference *	p<0.001*	p<0.001*	p<0.001*

355

356 Because two of the three spectral parameters were independent, the FLD values for the three
357 different parameter combinations had the same variance. Thus, the three normal distribution maps
358 of the three different parameter combinations were the same. As an example, the normal
359 distribution map of FLD value for the parameter combination (kI) between the malignant group
360 and normal group was plotted to evaluate its predictability as a classifier, as shown in **Fig. 6**.

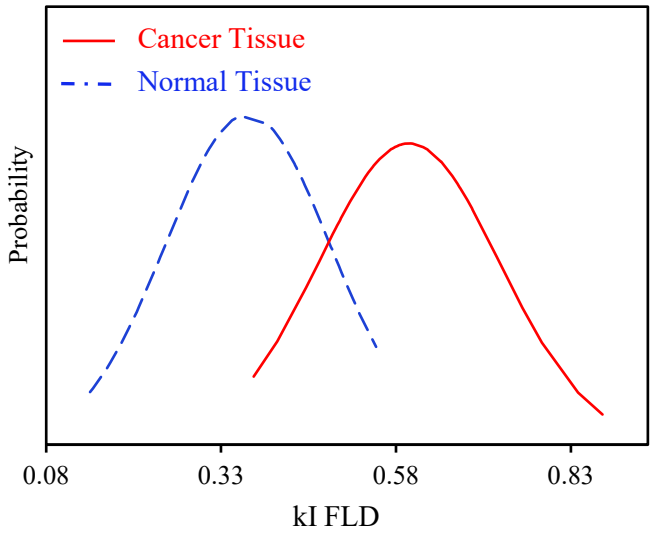

361

362 **Fig. 6.** The normal distribution of the FLD value for the spectral parameter combination (kI). The
363 red line and blue line represent the cancer and normal tissue group, respectively.

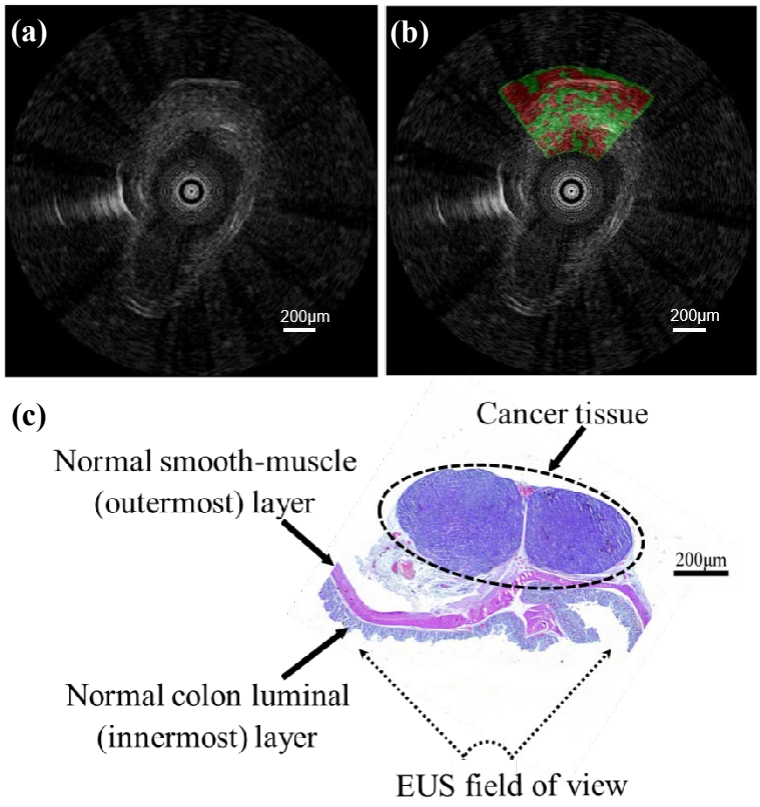

364

365 **Fig. 7.** (a) The B-mode image; (b) the combined image from the color-coded image and B-mode
366 image. The red color represents the cancer tissue region and the green color represents the water
367 or normal tissue region; (c) H/E histology image.

368

369 Finally, the value (kI FLD) for spectral parameter combination (kI) was selected as the classifier
370 to distinguish the malignant tissue from the normal tissue. The threshold of the value (kI FLD)
371 was set to be 0.48; if the value in the ROI was larger than 0.48, the corresponding region was
372 colored as red; if less than 0.48, the corresponding region was colored as green. The red color
373 region indicated the suspicious malignant tissue and the green color region indicated the water or
374 normal tissue. Each suspicious malignant tissue region was further determined regarding its
375 heterogeneous morphology and adjacent homogeneous morphology of the colon wall, as shown in

Fig. 7(a). In addition, the H/E histology images of the colon tissue segment containing tumor tissue were obtained. As a result, the combined image from the B-mode image and color-coded image was visually analyzed in comparison with the H/E histology image, as shown in **Fig. 7(b)-(c)**. Nevertheless, the perfect match between the combined image and the corresponding histology image was not able to be achieved because the tissue detachments during the microtome cutting process caused some morphological alternations to the histology specimen.

DISCUSSION

The abnormalities in the colorectal tract are not easy to differentiate in many cases, such as benign polyps, masses, colitis, Barrett's neoplasia and early cancerous lesions. The current diagnostic strategies in clinic, which are mainly based on the detection of morphological alterations, could be further improved by the emerging imaging modalities that could provide more comprehensive information of the tissue properties. The alternation conditions of the colorectal tract in the micro-structural and molecular level in addition to the morphological level are of great value. Nowadays, there is growing demand for the multi-modality imaging strategy to unmix the complexity of colorectal cancer (CRC).

In this report, the spectrum-based quantitative ultrasound (QUS) analysis of the ultrasound RF signals was implemented to characterize the colorectal malignancies based on a VX2 rabbit CRC model for the first time. To eliminate the response from the ultrasound electronic system and transducer, the ultrasound signals from colon tissue were calibrated. And, the resulting quasi-liner ultrasound spectra were fit by the linear regression test. As a result, three spectral parameters, including the slope (k), intercept (I) and Midband Fit (M), were obtained from the best-fit line.

The three spectral parameters were compared between the malignant tissue regions and adjacent normal tissue regions of the colon tissue specimen *ex vivo*. The mean Midband Fit (M) and intercept (I) showed significant differences between the malignant and normal tissue regions. The statistical analysis showed that there were significant differences in all the mean FLD values of the spectral parameter combinations (kI, kM and IM) (t test, $P < .05$). And, the combined image result from the B-mode image and color-coded image could visually correlate with the histology result. The combined image could not only depict the morphological changes, but also could show the micro-structural changes in the tissue property. When cancer was in progression, the early alternation was much potential to be in the molecular level which was not easy to be detected in clinic, while the morphological changes along with the micro-structural changes come much later. In this work, the color-coded EUS image along with the histology result showed the potential of this method by measuring the complementary morphological and micro-structural information simultaneously for better characterization of CRC. These results suggested that this method is potential to provide a novel quantitative method for characterization of the CRC by using the customized high-frequency endoscopic ultrasound (EUS) system.

The customized high-frequency EUS system made it possible to implement with other capable endoscopic imaging tools. The imaging characteristics such as the frequency spectrum of the transmitted pulse, the parameters of the receiver filter, the sampling rate, the number of scanning lines, and the length of scan line could all be configured flexibly. The novel image processing algorithms, such as tissue characterization algorithms based on the ultrasound radio-frequency (RF) signals, could be implemented into this customized high-frequency EUS system. The experiments on animal model of CRC showed that the mean FLD values of each two parameter combination

from the back-scattered ultrasound signals could provide a non-invasive method to quantitatively discriminate between malignant and normal colorectal tissues.

As to the limitations of this work, firstly, the animal model of VX2 CRC was limited because the inoculation positions had to be located at the smooth-muscle (outermost) layer of the rabbit colons due to the operation difficulty of transrectal implantation operation. In clinic, most early stage CRC began from the luminal (innermost) layer of the colorectal wall. Secondly, although the inherent compatibility of the high-frequency EUS system could make it suitable for complementing the routine endoscopy exam, the potential challenges for pre-clinical applications still exist, such as differentiating the sub-type dysplasia and individual variances. In the future, studies may combine other imaging modalities with this QUS method to further facilitate the development of the CRC characterization. Combining imaging modalities to form a dual- or multi-modality imaging strategy may leverage the strength of each modality and achieve a more comprehensive endoscopic procedure.

CONCLUSIONS

In this work, the quantitative ultrasound (QUS) based on the RF signals spectrum analysis was achieved in a VX2 rabbit colorectal cancer (CRC) model. The color-coded EUS result showed the potential of this method by measuring the complementary morphological and micro-structural information simultaneously. The results suggested that such endoscopic QUS method was potential to work as a novel complementary endoscopic tool for CRC characterization in the future.

ACKNOWLEDGEMENTS

The authors would like to thank Mr. Han Xu for the assistance of animal experiment, and Hong Kong Innovation and Technology Fund (ITS/053/16), Health and Medical Research Fund (03144266), National Natural Science Foundations of China (11674271, 11874382, and 11804357). The authors acknowledge the use of the University Research Facility in Life Sciences (ULS) and the Centre for Smart Materials of the Hong Kong Polytechnic University for the financial supports.

CONFLICT OF INTEREST STATEMENT

There is no conflict of interest that I should disclose.

REFERENCES

1. Messina CR. Barriers to Colorectal Cancer Screening: Patient, Physician, and System Factors. In: *Colorectal Cancer Screening*. Springer; 2011:57-66.
2. Hurlstone DP, Brown S, Cross SS, Shorthouse AJ, Sanders DS. High magnification chromoscopic colonoscopy or high frequency 20 MHz mini probe endoscopic ultrasound staging for early colorectal neoplasia: a comparative prospective analysis. *Gut*. 2005;54(11):1585-1589.
3. Hasan MK, Wallace MB. Image-enhanced endoscopy. *ASGE Clin Updat*. 2009;16(4):1-5.
4. Ferreira DS, Pinto VC, Correia JH, Minas G. Spectroscopic detection of gastrointestinal dysplasia using optical microsensors. *IEEE Trans Biomed Eng*. 2011;58(9):2633-2639.
5. Wallace MB, Kiesslich R. Advances in endoscopic imaging of colorectal neoplasia. *Gastroenterology*. 2010;138(6):2140-2150.
6. Kirtane TS, Wagh MS. Endoscopic optical coherence tomography (OCT): advances in gastrointestinal imaging. *Gastroenterol Res Pract*. 2014;2014.
7. Zipfel WR, Williams RM, Webb WW. Nonlinear magic: multiphoton microscopy in the biosciences. *Nat Biotechnol*. 2003;21(11):1369.
8. Yang J-M, Favazza C, Chen R, et al. Simultaneous functional photoacoustic and ultrasonic endoscopy of internal organs *in vivo*. *Nat Med*. 2012;18(8):1297.
9. Iddan G, Meron G, Glukhovsky A, Swain P. Wireless capsule endoscopy. *Nature*. 2000;405(6785):417.
10. Haji A, Ryan S, Bjarnason I, Donaldson N, Papagrigoriadis S. Colonoscopic high frequency mini-probe ultrasound is more accurate than conventional computed tomography in the

476 local staging of colonic cancer. *Color Dis*. 2012;14(8):953-959.
477 11. Hurlstone DP, Sanders DS, Lobo AJ, McAlindon ME, Cross SS. Prospective evaluation of
478 high-frequency mini-probe ultrasound colonoscopic imaging in ulcerative colitis: a valid
479 tool for predicting clinical severity. *Eur J Gastroenterol Hepatol*. 2005;17(12):1325-1331.
480 12. Kelly S, Harris KM, Berry E, et al. A systematic review of the staging performance of
481 endoscopic ultrasound in gastro-oesophageal carcinoma. *Gut*. 2001;49(4):534-539.
482 13. Waxman I, Saitoh Y, Raju GS, et al. High-frequency probe EUS-assisted endoscopic
483 mucosal resection: a therapeutic strategy for submucosal tumors of the GI tract. *Gastrointest*
484 *Endosc*. 2002;55(1):44-49.
485 14. Alves KZ, Soletti RC, de Britto MAP, et al. *In vivo* endoluminal ultrasound biomicroscopic
486 imaging in a mouse model of colorectal cancer. *Acad Radiol*. 2013;20(1):90-98.
487 15. Oelze ML, Mamou J. Review of quantitative ultrasound: Envelope statistics and backscatter
488 coefficient imaging and contributions to diagnostic ultrasound. *IEEE Trans Ultrason*
489 *Ferroelectr Freq Control*. 2016;63(2):336-351.
490 16. Feleppa EJ, Kalisz A, Sokil-Melgar JB, et al. Typing of prostate tissue by ultrasonic
491 spectrum analysis. *IEEE Trans Ultrason Ferroelectr Freq Control*. 1996;43(4):609-619.
492 17. Feleppa EJ, Liu T, Kalisz A, et al. Ultrasonic spectral-parameter imaging of the prostate.
493 *Int J Imaging Syst Technol*. 1997;8(1):11-25.
494 18. Feleppa EJ, Urban S, Kalisz A, Lizzi FL, Fair WR, Porter CR. Advanced ultrasonic imaging
495 of the prostate for guiding biopsies and for planning and monitoring therapy. In: *2000 IEEE*
496 *Ultrasonics Symposium. Proceedings. An International Symposium (Cat. No. 00CH37121)*.
497 Vol 2. IEEE; 2000:1399-1403.
498 19. Feleppa EJ. Ultrasonic tissue-type imaging of the prostate: implications for biopsy and

499 treatment guidance. *Cancer biomarkers*. 2008;4(4-5):201-212.
500 20. Oelze ML, Zachary JF, O'Brien Jr WD. Differentiation and characterization of mammary
501 fibroadenomas and 4T1 Carcinomas using ultrasound parametric imaging. *IEEE Trans Med*
502 *Imag*. 2004;23(6):764-771.
503 21. Lizzi FL, Astor M, Liu T, Deng C, Coleman DJ, Silverman RH. Ultrasonic spectrum
504 analysis for tissue assays and therapy evaluation. *Int J Imaging Syst Technol*. 1997;8(1):3-
505 10.
506 22. Saegusa-Beecroft E, Machi J, Mamou J, et al. Three-dimensional quantitative ultrasound
507 for detecting lymph node metastases. *J Surg Res*. 2013;183(1):258-269.
508 23. Mamou J, Coron A, Oelze ML, et al. Three-dimensional high-frequency backscatter and
509 envelope quantification of cancerous human lymph nodes. *Ultrasound Med Biol*.
510 2011;37(3):345-357.
511 24. Mamou J, Coron A, Hata M, et al. Three-dimensional high-frequency characterization of
512 cancerous lymph nodes. *Ultrasound Med Biol*. 2010;36(3):361-375.
513 25. Oosterveld BJ, Thijssen JM, Hartman PC, Romijn RL, Rosenbusch GJE. Ultrasound
514 attenuation and texture analysis of diffuse liver disease: methods and preliminary results.
515 *Phys Med Biol*. 1991;36(8):1039.
516 26. Ghoshal G, Lavarello RJ, Kemmerer JP, Miller RJ, Oelze ML. *Ex vivo* study of quantitative
517 ultrasound parameters in fatty rabbit livers. *Ultrasound Med Biol*. 2012;38(12):2238-2248.
518 27. Lee DJ, Sigel B, Swami VK, et al. Determination of carotid plaque risk by ultrasonic tissue
519 characterization. *Ultrasound Med Biol*. 1998;24(9):1291-1299.
520 28. Spencer T, Ramo MP, Salter DM, et al. Characterisation of atherosclerotic plaque by
521 spectral analysis of intravascular ultrasound: an *in vitro* methodology. *Ultrasound Med Biol*.

1997;23(2):191-203.

29. Huang CC, Zhou Q, Ameri H, et al. Determining the acoustic properties of the lens using a high-frequency ultrasonic needle transducer. *Ultrasound Med Biol*. 2007;33(12):1971-1977.

30. Huang CC, Ameri H, DeBoer C, et al. Evaluation of lens hardness in cataract surgery using high-frequency ultrasonic parameters in vitro. *Ultrasound Med Biol*. 2007;33(10):1609-1616.

31. Qiu W, Yu Y, Tsang FK, Sun L. An FPGA-based open platform for ultrasound biomicroscopy. *IEEE Trans Ultrason Ferroelectr Freq Control*. 2012;59(7):1432-1442.

32. Qiu W, Chen Y, Li X, et al. An open system for intravascular ultrasound imaging. *IEEE Trans Ultrason Ferroelectr Freq Control*. 2012;59(10):2201-2209.

33. Liu C, Sun L, Chen Y, Dai J, Qiu W. A novel high-frequency endoscopic ultrasound system for colorectal cancer diagnosis. In: *2013 IEEE International Ultrasonics Symposium (IUS)*. IEEE; 2013:2045-2048.

34. Liu C, Yang Y, Sun L, Huang C-C. Characterization of the colorectal cancer in a rabbit model using quantitative high-frequency endoscopic ultrasound. In: *2013 IEEE International Ultrasonics Symposium (IUS)*. IEEE; 2013:891-894.

35. Liu C. Characterization of the colorectal cancer by combining high-frequency endoscopic ultrasound and quantitative ultrasound. 2014.

36. Lizzi FL, Feleppa EJ, Alam SK, Deng CX. Ultrasonic spectrum analysis for tissue evaluation. *Pattern Recognit Lett*. 2003;24(4-5):637-658.

37. Lizzi FL, Greenebaum M, Feleppa EJ, Elbaum M, Coleman DJ. Theoretical framework for spectrum analysis in ultrasonic tissue characterization. *J Acoust Soc Am*. 1983;73(4):1366-1373.

545 38. Lizzi FL, Astor M, Feleppa EJ, Shao M, Kalisz A. Statistical framework for ultrasonic
546 spectral parameter imaging. *Ultrasound Med Biol*. 1997;23(9):1371-1382.
547 39. Lizzi FL, Astor M, Coleman DJ, Silverman RH, Reinstein DZ. Very-high frequency
548 ultrasonic imaging and spectral assays of the eye. In: *Acoustical Imaging*. Springer;
549 1997:107-112.